Dual wavelength Raman lidar observation of tropical high-altitude cirrus clouds during the ALBATROSS 1996 campaign

Georg Beyerle,[1,2] Jürgen Schafer,[2] Roland Neuber,[2] Otto Schrems,[2] I. Stuart McDermid[1]

Short title: LIDAR OI3SERVATIONS OF TROPICAL CIRRUS CLOUDS

[1] Jet Propulsion Laboratory, California Institute of Technology, Wright wood, CA

[2] Alfred Wegener Institute for Polar and Marine Research, Bremerhaven and Pot sdam, Germany

Abstract. Dual wavelength Raman lidar observations of tropical high-altitude cirrus clouds were performed during the ALBATROSS 1996 campaign aboard the German research vessel "POLARSTERN" on the Atlantic ocean in October–November 1996. On the basis of 475 observations bet ween 23.5°N and 23.5° S we find in 72% of the altitude profiles indications of the presence of cirrus cloud layers. About one-third of the detected cirrus layers are subvisible with an optical thickness of less than 0.03 at a wavelength of 532 nm. Effective particle radii ranging from 3 to 200 μm are derived with 11 % of the measurements showing values larger than 50 μm. Subvisible clouds are found to contain primarily particles as large as 100 pm. Rapid sedimentation of these large particles may contribute significantly to the dehydration process in the upper troposphere.

1. Introduction

The frequent occurrence of high-altitude cirrus clouds at tropical latitudes is well known from satellite observations [*Prabhakara et al., 1988; Wang et al.,* 1994]. Because of their ubiquitous nature and global distribution these cloud layers can significantly affect the radiation budget of the atmosphere [e.g., Stephens *et al.*, 1990]. Furthermore, as tropospheric air enters the stratosphere predominantly in the tropics by upward transport the formation of tropical cirrus layers can influence the stratospheric water vapour content [*Danielsen*, 1993; *Potter and Holton*, 1995; *Jensen et al.*, 1996*b*]. Recently, *Jensen et al.* [1996a] have performed model calculations which indicate that cirrus layers can form by slow large-scale vertical motions leading to the formation of large particles with effective radii exceeding 10–20 pm. These particles precipitate rapidly and may reduce water vapour mixing ratios by as much as 1 ppmv near the tropical tropopause.

In this paper we present results from lidar observation of tropical visible and subvisible cirrus clouds above the Atlantic ocean during the ALBATROSS campaign (Atmospheric chemistry and lidar studies above the Atlantic ocean related to ozone and other trace gases in the tropo- and stratosphere). The measurements were performed with a mobile aerosol Raman lidar aboard the German research vessel "POLARSTERN" during a cruise from Bremerhaven, Germany (53.6°N, 8.6°E) to Punta Quills, Argentina (50.2°S, 68.3°W) in October-November 1996. Based on 107 hours of observations at tropical and subtropical latitudes we estimate the frequency of occurrence of optically thin cirrus layers and derive particle size distributions.

2. Instrumentation and data reduction

The aerosol Raman lidar instrument transmits simultaneously at wavelengths of 355 and 532 nm with a pulse repetition frequency of 30 Hz. Maximum pulse energies

are 300 mJ at both wavelengths. Elastic and inelastic components of the backscattered light due to molecular and aerosol scattering and due to vibrational Raman scattering on molecular nitrogen, respectively, at altitudes between 5 and 50 km are detected. Additionally, the instrument includes detection channels for cross-polarized return signals at 355 and 532 nm. Typically, counts from about 12,000 laser pulses are summed to produce a backscatter profile with 7.5 or 120 m altitude resolution. The instrument operated during night-time only. Further technical details are given in *Schäfer et al.* [1995].

'l'he raw data are corrected for photodetector saturation, deadtime effects and background noise. In the following $\beta^{A,M}(z,\lambda)(\alpha^{A,M}(z,\lambda))$ denotes the backscatter (extinction) coefficient for aerosol and molecular scattering as a function of altitude z and wavelength λ, respectively. Backseat ter rat io $R = \beta^A/\beta^M + 1$ is derived from the corrected elastic and inelastic return signals, P(z, λ) and $P(z,\lambda^R)$, by

$$R(z) = k\,\frac{P(z,\lambda^R)}{P(z,\lambda)}\,\exp\int_{z_s}^{z} d\tilde{z}\,\left(\alpha^M(\tilde{z},\lambda) - \alpha^M(\tilde{z},\lambda^R)\right).$$

Here, $\lambda^R = (\lambda^{-1} - 2329.66\ \text{cm-l})^{-1}$ denotes the N_2 Raman shifted wavelength and z_s is the altitude of the lidar instrument. The value of k is obtained by normalizing R to unity at an aerosol free altitude range between 16 and 18 km. As cirrus ice particles in general are large compared to the lidar wavelength we ignore the wavelength dependence of α^A. Volume depolarization δ is given by

$$\delta = \frac{\beta_\perp^M + \beta_\perp^A}{\beta_\parallel^M + \beta_\parallel^A}.$$

The subscripts $\parallel$ and $\perp$ denote the aligned- and cross-polarized component, respectively. δ is normalized to $\delta^M \equiv 0.014$ at an aerosol free altitude range between 16 and 18 km [*Young*, 1980]. We obtain the optical thickness τ between altitudes z_b = 11 km and z_t = 16 km from the inelastic return signals $P(z,\lambda^R)$ by

$$\tau(z_b, z_t, \lambda, \lambda^R) = \frac{1}{2}\ \text{in}\ \left(\frac{P(z_b,\lambda^R)\,(z_b - z_s)^2\,N(z_t)}{P(z_t,\lambda^R)\,(z_t - z_s)^2\,N(z_b)}\right)$$

$$-\frac{1}{2}\int_{z_b}^{z_t} dz\,(\alpha^M(\lambda)+\alpha^M(\lambda^R))$$

where $N(z)$ denotes the molecular number density and is obtained from daily serological balloon soundings aboard "PO LARSTERN". Strictly, τ is the arithmetic mean of optical thicknesses at λ and λ^R. In the following we will refer to τ as optical thickness at wavelength λ. As will be shown later τ is typically much smaller than unity. Therefore, *we* assume that contributions from multiple scat tering processes can be ignored.

Figure 1.

3. Results and discussion

During the ALBATROSS campaign lidar measurements were performed on the Atlantic ocean between 35°N and 45°S latitude and 25"W and 30"W longitude. The following discussion is restricted to the tropical and subtropical observations (30°N–30°S). The observations took place on 11 nights between October 18 and October 31, 1996; total measurement time was 107 hours.

In general we observed a high temporal variability and spatial inhomogeneity of tropical cirrus cloud layers. An example is shown in Figure 1 which gives a time series of altitude profiles of R at 355 nm recorded between 21:17 and 21:59 UTC on October 21, 1996 at 11 .99°N and 28.25° W. Each profile corresponds to a measurement period of 34 seconds with an altitude resolution of 7.5 m. The cirrus cloud top is located a few hundred meters below the tropopause altitude which is obtained by linear temporal interpolation of radio sonde data. However, the exact tropopause altitude is uncertain as the sonde launches occurred 9 hours before and 15 hours after the lidar observation. Throughout the campaign cirrus top layers are observed in close vicinity to and below the tropopause altitude. There is no indication of cloud formation above the tropopause in the lower stratosphere.

Figure 2.

The presence of optically thin cirrus cloud layer is more readily detected in terms of changes in volume depolarization δ than in backscatter ratio R as is shown in Figure 2.

Figure 2 gives the maximum value of backscatter ratio (volume depolarization) in the altitude interval 11 to 16 km denoted by R_{max} (δ_{max}) as a function of the optical thickness at 532 nm. Values of τ below about 0.01 are increasingly sensitive to the statistical noise of the N_2 Raman return signal and their errors grow correspondingly. Vertical lines indicate the subvisibility threshold τ = O.O3 of cirrus clouds introduced by *Sassen et al.* [1989]. Typically, R_{max} of a subvisible cirrus does not exceed values of 2–3 whereas in terms of δ_{max} a clear separation between presence of subvisible clouds (δ_{max} >0.02, τ < 0.03) and a clear sky condition (δ_{max} = 0.014) can be seen. Based on all available data at tropical latitudes with δ_{max} >0.02 we find that about 50% of the observed cirrus layers are subvisible.

Figure 3.

Figure 3 summarizes the frequency of cirrus cloud occurrence in our data set. It shows the relative frequency of occurrence of δ_{max} at 23.5°S–23.5°N (top) and 23.5 -30° S / 23.5–30°N (bottom). In the tropics we find in 72% out of 475 profiles maximum volume depolarizations exceeding 0.02. In the subtropics this percentage reduces to 36% based on 157 profiles. Furthermore, in subtropical clouds lower values of δ are observed in general. The following analysis of particle size distributions is based solely on data recorded between 23.5° S and 23.5"N.

In order to obtain information on particle sizes we derive estimates of the particle size distribution from the observed colour ratio $C(z,\lambda_1,\lambda_2) = (R(z,\lambda_1)-1)/(R(z,\lambda_2)-1)$ where λ_1 = 355 nm and λ_2 = 532 nm. The particle size distribution is assumed to follow a power law

$$\frac{dn}{dr} = AT\text{-}B \qquad r_a \leq r \leq r_b$$

with parameters A, B, r_a = 1 pm, and r_b = 500 μm [*Heymsfield and Platt, 1984*]. Within the framework of Mie scattering theory we obtain a calculated backscatter coefficient $\tilde{\beta}^A(\lambda) = \pi A \int_{r_a}^{r_b} dr\, r^{2-B} Q_\pi(x, m(\lambda))$ and the parameter B can be derived

numerically from the relation

$$C(2, \lambda_1, \lambda_2) \approx \frac{\int_{r_a}^{r_b} dr\ r^{2-B}\, Q_\pi(x, m(\lambda_1))\, \lambda_1^{4.08}}{\int_{r_a}^{r_b} dr\ r^{2-B}\, Q_\pi(x, m(\lambda_2))\, \lambda_2^{4.08}} \quad (6)$$

The backscatter efficiency Q_π of a particle with size parameter $x = 2\pi r/\lambda$ and refractive index m is calculated numerically [*Bohren and Huffman, 1983*]. For water ice $m = 1.325 + i3.76 \cdot 10^{-9}$ and $1.312 + i3.11 \cdot 10^{-9}$, at 355 and 532 nm, respectively [Warren, 1984]. The wavelength exponent 4.08 takes into account atmospheric dispersion [*Ciddor*, 1996]. Finally, parameter A follows from

$$A = \frac{\beta^A(\lambda)}{\pi \int_{r_a}^{r_b} dr\ r^{2-B}\, Q_\pi(x, m(\lambda))} \quad (7)$$

Figure 4.

We are aware of the apparent conflict between the use of Mie scattering theory which is valid for spherical particles only and the nonspherical characteristics of cirrus ice particles. In order to estimate the systematic error due to the use of Mie theory cross-sectional area densities

$$\mathcal{S} = \pi A \int_{r_a}^{r_b} dr\ r^{2-B}$$

derived from our algorithm are compared with a parameterization given by *Sassen et al.* [1989]

$$\tilde{\mathcal{S}} = \frac{\beta^A(\lambda = 694\ \text{nm})}{9} \quad (8)$$

Values of g at a wavelength of 694 nm are 0.052, 0.172, and 0.076 for thin plate crystals, thick plate crystals, and long column crystals, respectively [*Sassen et al.*, 1989]. For simplicity we use the mean value, g = (0.052 + 0.172 + 0.076)/3 = 0.1 $\pm$ 0.06 and assume that the parameterization is valid at 532 nm, as well. The comparison between $\tilde{\mathcal{S}}$ and $\mathcal{S}$ is shown in figure 4. The standard deviation of (S — S)/S is 23%, the maximum value is 34%. Under the assumption that the errors scale with the effective particle radius r_e we estimate the systematic error of r_e to be 12% and the systematic error of volume density

$$V = \frac{4\pi}{3} A \int_{r_a}^{r_b} dr\ r^{3-B}$$

to be 35%. Figure 5.

We define an effective particle radius r_e by forming the ratio of volume density V and the cross-sectional area density $\mathcal{S}$,

$$r_e \equiv \frac{3}{4}\frac{V}{\mathcal{S}} .$$

The correlation of r_e with the aerosol backscatter coefficient at 532 nm is given in Figure 5. For comparison the range of corresponding molecular backscatter coefficients at 532 nm is marked as a grey area. Figure 5 shows that particles exhibiting low values of β^A predominantly have large effective radii of about 100 pm. As will be discussed in the next paragraph these large particles which are difficult to detect by remote sensing instruments contain a considerable fraction of the available water in the upper troposphere. Figure 6.

From V and the ice mass density ρ_i = 0.78 g/cm^3 we calculate the H_2O equivalent volume mixing ratio $(\text{evmr})x = N_A \rho_i V / M_{H_2O} / N$ where N_A and M_{H_2O} = 18.01 g/mole denote the Avogadro number and the molar mass of water, respectively. 1.e. evmr is the increase in water volume mixing ratio that would be observed if all H_20 molecules in the liquid or solid phase were present in the gas phase. The water evmr of cirrus particles with effective radii r_e is plotted in Figure 6a. In contrast, Figure 6b gives the fraction of water evmr which is contained in particles with radii exceeding 50 pm. Comparison between Figure 6a and b shows little difference for effective radii larger than about 10-20 pm. This suggests that in particle size distributions with r_e < 10-20 μm the major fraction of the available water is contained in particles smaller than 50 pm. As ice particles larger than 50 μm have fall speeds exceeding 1 km per hour [*Pruppacher and Klett*, 1978] Figure 6b indicates the fraction of 11_20 evmr which may be removed from the upper troposphere by rapid sedimentation of cirrus ice particles. We conclude that cloud layers with effective radii smaller than about 10-20 μm do not contribute significantly to the dehydration process. However, subvisible cirrus clouds with low

values of $\beta_{\lambda} \approx 10^{-7}\ m^{-1}\ sr^{-1}$ predominantly exhibit effective radii of about 100 μm and water evmr between 0.1 and 1 ppmv are contained in rapidly sedimenting ice particles.

Our observations substantiate the interpretations by *Jensen et al. [1996a]* of their model calculations that subvisible cirrus layers formed by slow large-scale vertical upward motions lead to the formation of large particles with radii larger than 20 μm which precipitate rapidly and contribute significantly to the dehydration process in the upper tropical troposphere. The frequent occurrence of subvisible cirrus during our campaign suggests that this removal process contributes significantly to the stratospheric water budget. Clearly, further lidar observations at tropical latitudes are needed in order to extend and improve the data base required for this type of analysis.

Acknowledgments. The help and support by the crew of "POLARSTERN" during the ALBATROSS campaign is gratefully acknowledged. We thank P. Rairoux for stimulating discussions and R. Weller and J. Gräser for providing the radio sonde data. The MARL lidar instrument was designed and built by OHB System Bremen, Germany in co-operation with Alfred Wegener Institute, Bremerhaven and Potsdam, Germany and GKSS Forschungszentrum Geesthacht, Germany. We gratefully acknowledge financial support for this project by Deutsche 13undesstiftung Umwelt, Germany. G. B. thanks the National Research Council for the award of an associateship. Part of the work described here was performed at the Jet Propulsion Laboratory, California Institute of Technology, through an agreement with the National Aeronautics and Space Administration. Contribution 1245 of the Alfred Wegener Institute.

References

Bohren, C. F., and D. R. Huffman, *Absorption and* scattering *of light by small particles,* John Wiley & Sons, New York, 1983.

Ciddor, P. E., Refractive index of air: new equations for the visible and near infrared, *Appl. Opt.,* 35, (9), 1566-1573, 1996.

Danielsen, E. F., In situ evidence of rapid, vertical, irreversible transport of lower tropospheric air into the lower stratosphere by convective cloud turrets and by large-scale upwelling in tropical cyclones, *J. Geophys. Res.,* 98, (D5), 8665–8681, 1993.

Heymsfield, A. J., and C. M. R. Platt, A parameterization of the particle size spectrum of ice clouds in terms of the ambient temperature and ice water content, *J. Atmos. Sci., 41,* 846-855, 1984.

Jensen, E. J., O. B. Toon, L. Pfister, and H. B. Selkirk, Dehydration of the upper troposphere and lower stratosphere by subvisible cirrus clouds near the tropical tropopause, *Geophys. Res. Lett.,* 23, (8), 825-828, *1996a.*

Jensen, E. J., O. B. Toon, H. B. Selkirk, J. D. Spinhirne, and M. R. Schoeberl, On the formation and persistence of subvisible cirrus clouds near the tropical tropopause, *J. Geophys. Res., 101,* (D16), 21361-21375, *1996b.*

Potter, B. E., and J. R. Holton, The role of monsoon convection in the dehydration of the lower tropical stratosphere, *J. Atmos. Sci.,* 52, (8), 1034-1050, 1995.

Prabhakara, C., R. S. Fraser, G. Dalu, M. C. Wu, R. J. Curran, and T. Styles, Thin cirrus clouds: Seasonal distribution over oceans deduced from Nimbus-4 IRIS, *J. Appl. Meteorol.,* 27, 379-399, 1988.

Pruppacher, H. P., and J. D. Klett, *Microphysics of clouds and precipitation,* D. Reidel Publ., Dordrecht, 1978.

Sassen, K., M. K. Griffin, and G. C. Dodd, Optical scattering and microphysical properties of subvisual cirrus clouds, and climatic implications, *J. Appl. Meteorol., 28, 91-98, 1989.*

Schafer, H.-J., O. Schrems, G. Beyerle, B. Hofer, W. Mildner, F. A. Theopold, W. Lahmann, C. Weitkamp, and M. Steinbach, A modular and mobile multi-purpose lidar system for observation of tropospheric and stratospheric aerosols, *SPIE EurOpto series, 2581, 128-136, 1995.*

Stephens, G. L., S. C. Tsay, P. W. Stackhouse, and P. J. Flatau, The relevance of the micro-physical and radiative properties of cirrus clouds to climate and climate feedback, *J. Atmos. Sci.*, 47, 1742-1753, 1990.

Wang, P.-H., M. P. McCormick, L. R. Poole, W. P. Chu, G. K. Yue, G. S. Kent, and K. M. Skeens, Tropical high cloud characteristics derived from SAGE II extinction measurements, *Atmospheric Research, 34,* 53-83, 1994.

Warren, S. G., Optical constants of ice from the ultraviolet to the microwave, *Appl. Opt., 23, (8), 1206-1225,1984.*

Young, A. T., Revised depolarization correction for atmospheric extinction, *Appl. Opt., 19, (20), 3427-3428,1980.*

G. Beyerle and I. S. McDermid, Table Mountain Facility, Jet Propulsion Laboratory, California Institute of Technology, P.O.B. 367, Wrightwood, CA 92397. (e-mail: beyerle@tmf.jpl.nasa.gov; mcdermid@tmf.jpl.nasa.gov)

J. Schafer and O. Schrems, Alfred Wegener Institute, P.O.B. 120161, D-27515 Bremerhaven, Germany. (e-mail: jschafer@awi-bremerhaven.de; ottoschrems@awi-bremerhaven.de)

R. Neuber, Alfred Wegener Institute, P.O.B. 600149, D-14401 Potsdam, Germany. (e-mail: neuber@awi-potsdam.de)

Received XXX; revised XXX; accepted XXX.

To appear in *Journal of Geophysical Research, 1997.*

This manuscript was prepared with AGU's LaTeX macros v4, with the extension package 'AGU++' by P. W. Daly, version 1.5b from 1996/10/24.

Figure Captions

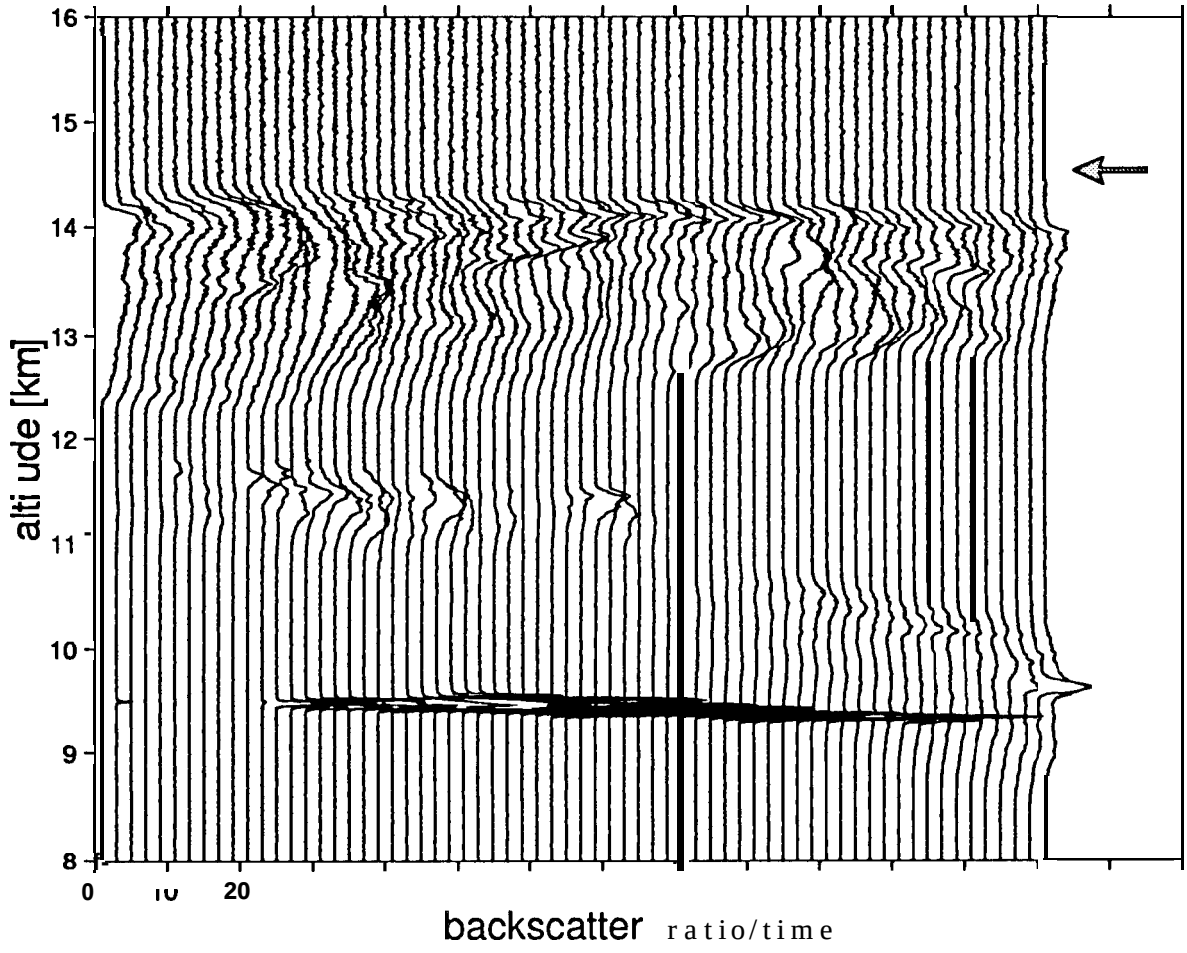

Figure 1. Temporal variability of cirrus clouds layer during a time period of 37 min on October 21, 1996 at 11.99°N latitude and 28.25°W longitude. A time series of backscatter ratio at 355 nm is shown. Temporal and spatial resolutions are 34 seconds and 7.5 m, respectively. The thin aerosol layer at 9.5 km is probably caused by an aircraft contrail. For clarity, profiles are separated by 2 units. The arrow indicates the tropopause altitude.

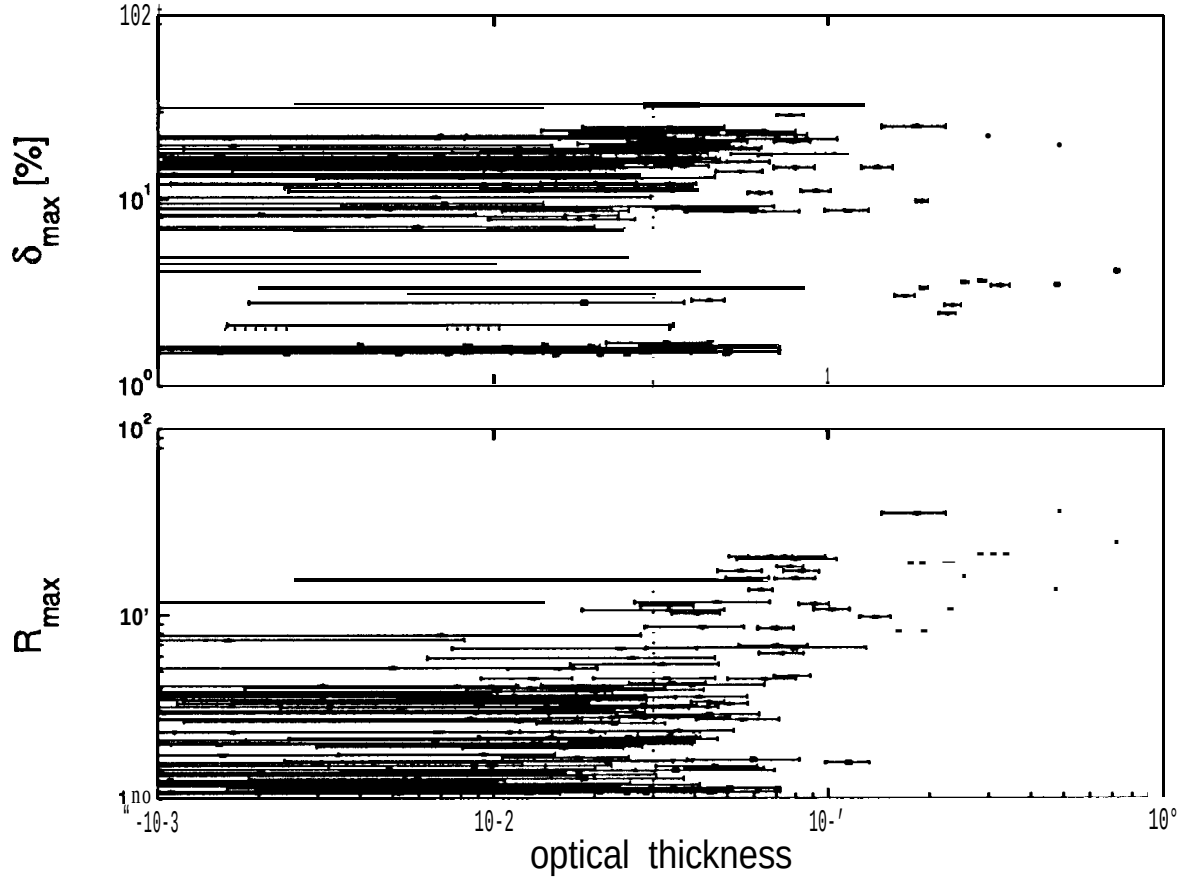

Figure 2. Maximum volume depolarization (top) and maximum backscatter ratio (bottom) as a function of optical thickness at a wavelength of 532 nm. The vertical dashed lines indicate the subvisibility threshold τ = 0.03.

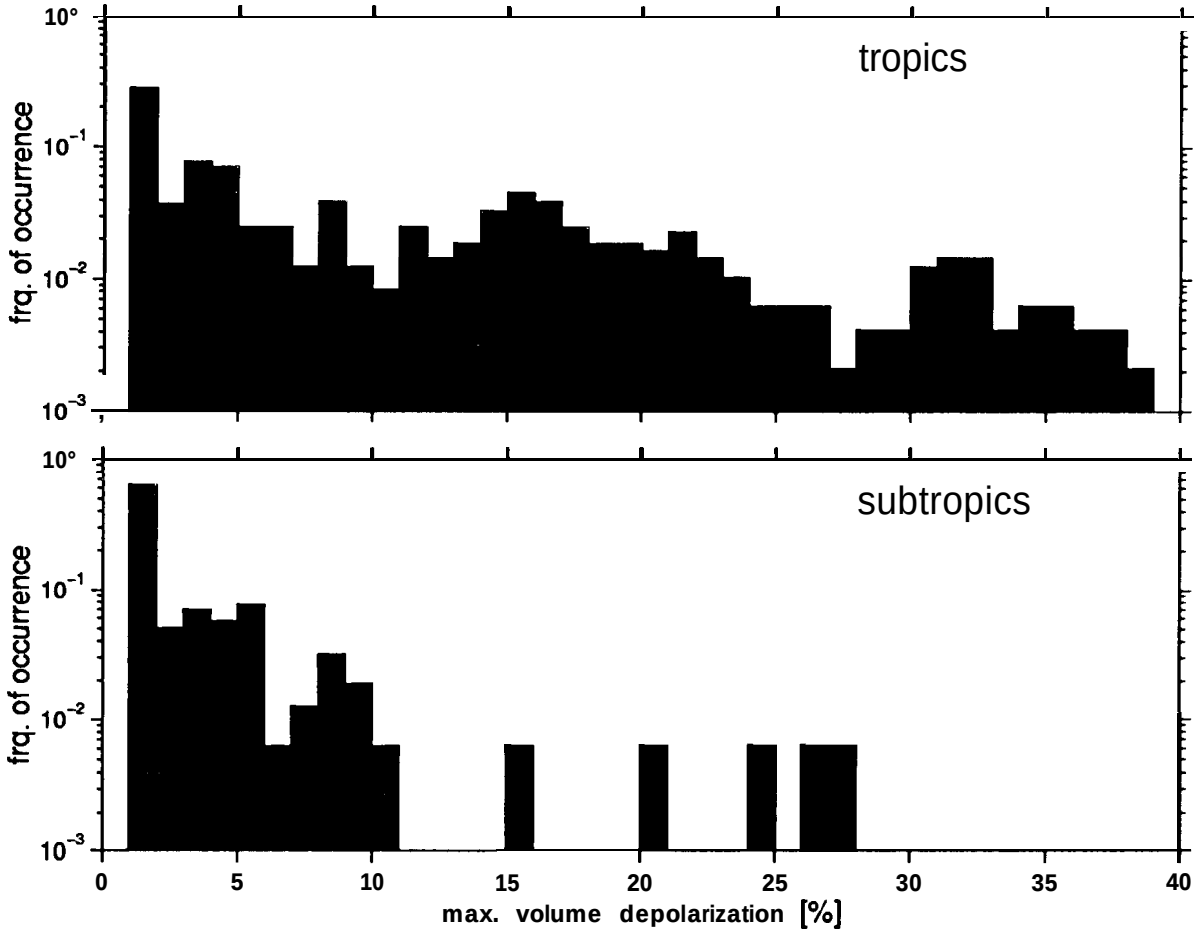

Figure 3. Relative frequency of occurrence of maximum volume depolarization in the 11 to 16 km altitude range between 23.5°S–23.5°N (top) and 23.5 °–300N/S (bottom). Note the logarithmic scale.

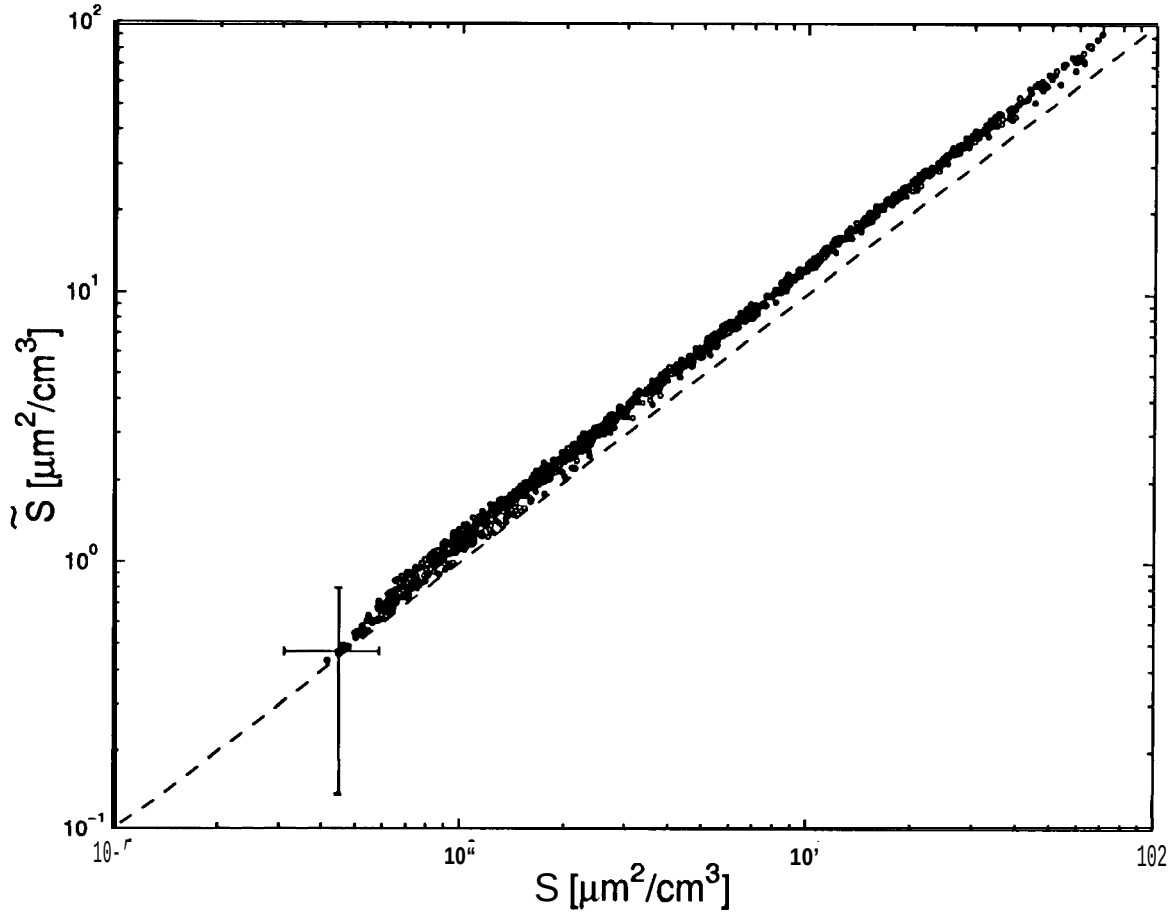

Figure 4. Comparison between the calculated cross-sectional area density $(\mathcal{S})$ and the pararneterization $(\tilde{\mathcal{S}})$ by *Sassen et al. [1989].* The dashed line gives $\mathcal{S}$ = S. For clarity errors are shown for one data point only.

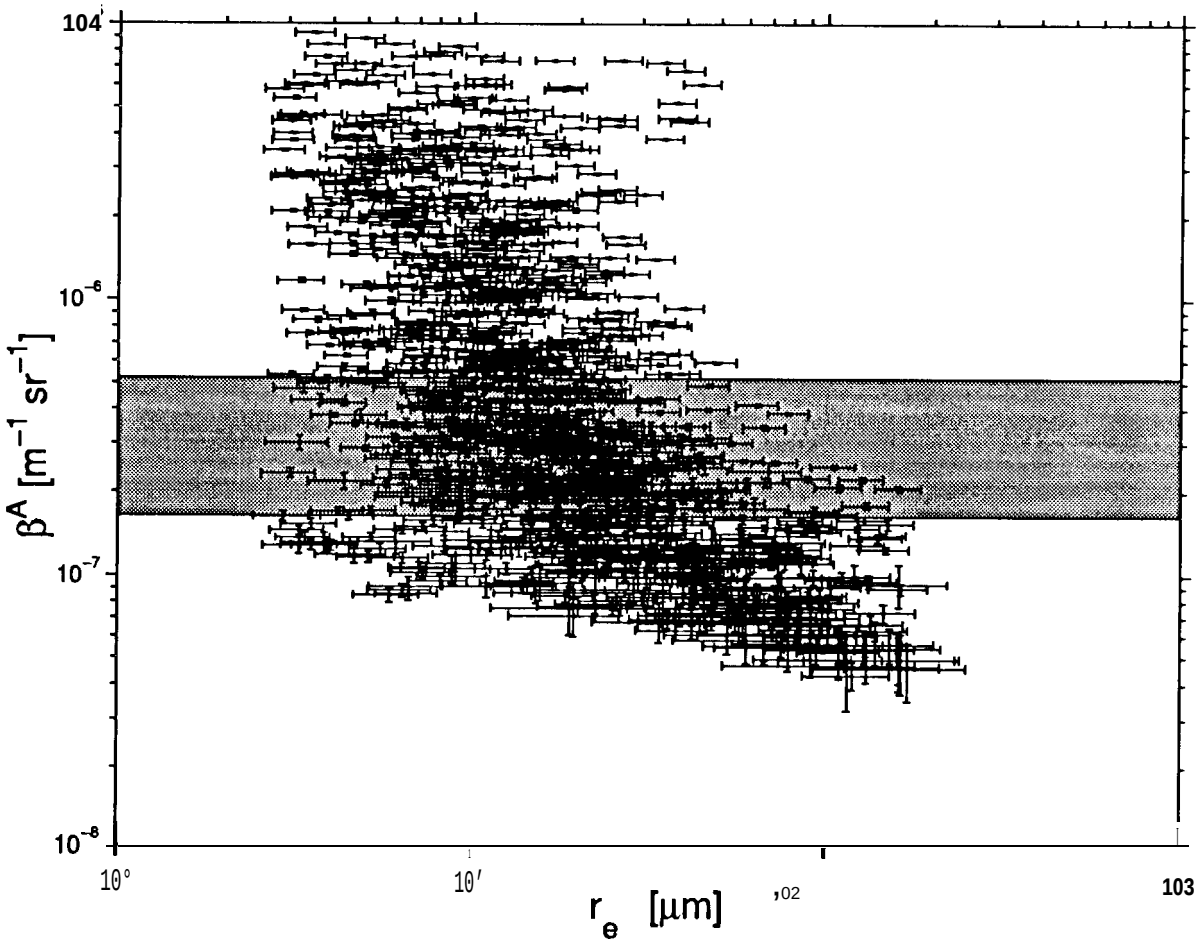

Figure 5. Aerosol backscatter coefficient at 532 nm as a function of effective particle radius. The range of values of the corresponding molecular backscatter coefficient at 532 nm is marked in grey.

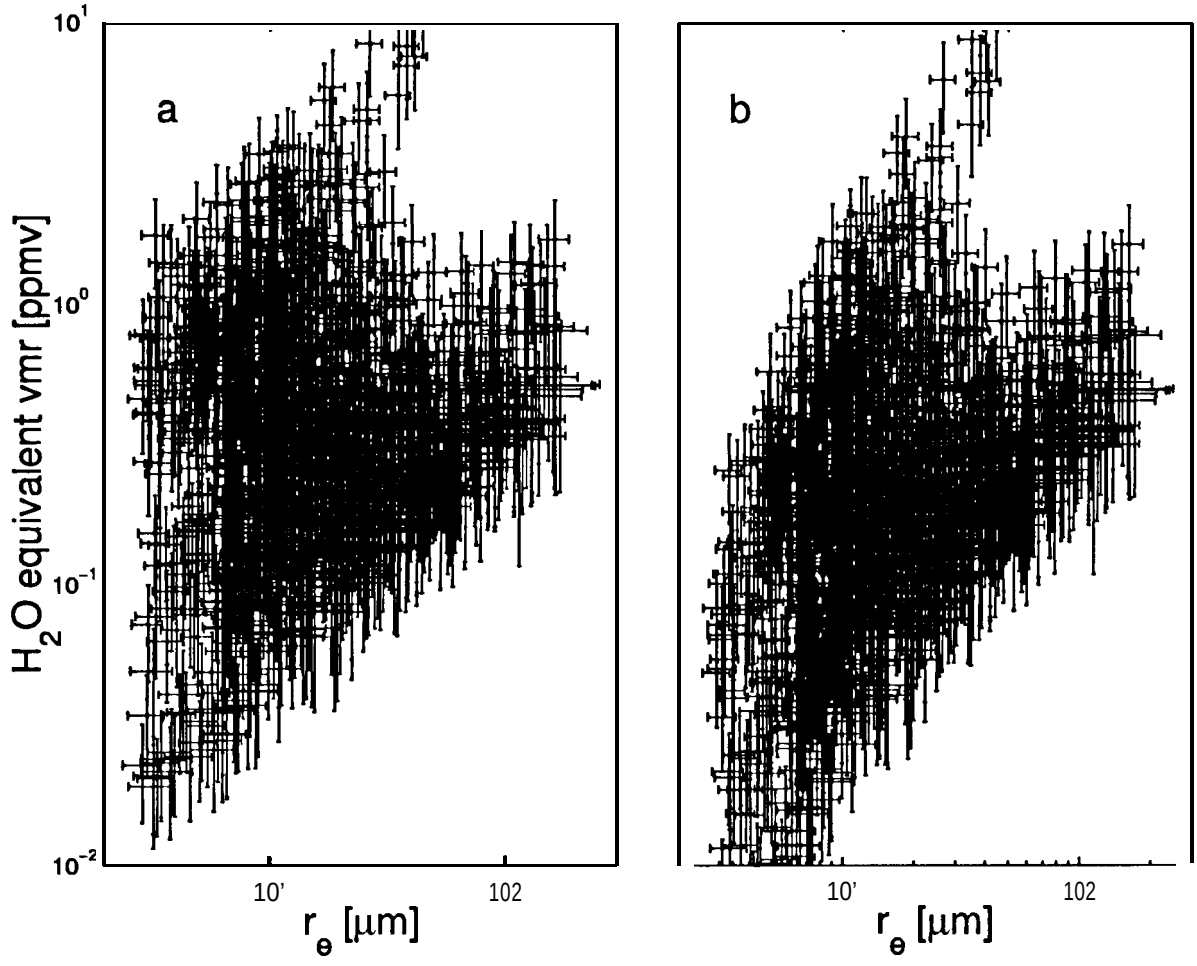

Figure 6. H_2O equivalent volume mixing ratio as a function of effective radius (left) and the fraction of equivalent vmr contained in particles with radii larger than 50 μm (right).